



# Correlation between CuO and CoO nanoparticles concentration and magnetic reversal in mechanochemically prepared cordierite ceramics

Karla Čech Barabaszová<sup>a,\*</sup>, Jana Kupková<sup>a,2</sup>, Kamila Hrabovská<sup>b,3</sup>, Sylva Holešová<sup>a,4</sup>, Agnieszka Antończyk<sup>a,c,5</sup>

<sup>a</sup> Nanotechnology Centre, CEET, VSB - Technical University of Ostrava, 17. listopadu 15/2172 Poruba, Ostrava 708 00, Czech Republic

<sup>b</sup> Department of Physics, VSB - Technical University of Ostrava, 17. listopadu 15/2172 Poruba, Ostrava 708 00, Czech Republic

<sup>c</sup> Department of Biomaterials and Medical Devices Engineering, Faculty of Biomedical Engineering, Silesian University of Technology, Roosevelta 40 st., Zabrze 41-800, Poland

## ARTICLE INFO

### Keywords:

Cordierite nanocomposite particles  
CuO and CoO nanoparticles  
Magnetic properties  
Structural  
Surface and phase changes

## ABSTRACT

Cordierite nanocomposite particles doped with CuO and CoO nanoparticles at different concentrations were prepared using a mechanochemical method involving grinding and sintering processes. The morphology of cordierite nanocomposite particles was studied using scanning electron microscopy (SEM) and phase changes were evaluated using X-ray diffraction (XRD) analysis. The particles size (PS) changes were expressed by two mode diameters ( $d_{m1}$  and  $d_{m2}$ ) that confirmed the bimodal character of the particle size distributions except for C5.5\_CuO and C5.5\_CoO samples. Decreasing of the  $\zeta$ -potential was evaluated with the increasing concentration of nanoparticles which corresponds to the agglomeration of the fine particles. All XRD patterns showed the formation of indialite in original cordierite and in cordierite nanocomposites enriched about CuO and CoO nanoparticles. The addition of metal oxides to the cordierite pre-ceramic mixtures led to the creation of two spinel-type oxides ( $\text{CuAl}_2\text{O}_4$  and  $\text{CoAl}_2\text{O}_4$ ). Changes in metal oxide concentration were evaluated using XRF analysis. These changes corresponded to magnetic reversal at low magnetic fields originating from pure cordierite ceramics and a linear contribution at higher magnetic fields, which increased systematically with the content of doped nanoparticles. The formation of spinel phase and spinel-type oxides was also confirmed by analysis of cordierite pre-ceramic mixtures by TGA.

## 1. Introduction

The ever-increasing interest in nanostructured materials means there is a need to find new, useful properties in materials that have previously been used. One such material is cordierite ceramics, which has recently become more popular due to its simple preparation and natural origin. Modifying its chemical composition with suitable nanostructured fillers therefore makes it a key component in new nanocomposite materials.

Cordierite ( $2\text{MgO} \cdot 2\text{Al}_2\text{O}_3 \cdot 5\text{SiO}_2$ ) is a well-known magnesium aluminum silicate mineral. Its structure is characterized by six-

membered rings consisting of  $\text{SiO}_4$  and  $\text{Al}_4\text{O}$  tetrahedral rings. These rings are formed by either four or six cation member rings [1–3]. Cordierite is an attractive ceramic material with variety of applications, mainly due to its good thermal and chemical stability, low thermal expansion coefficient, low dielectric constant, excellent thermal shock resistance and high refractoriness and good mechanical properties [1,2].

The typical synthesis method for cordierite ceramics involves high temperature sintering (1340 – 1450 °C) of the pre-ceramic mixtures containing individual oxides ( $\text{MgO}$ ,  $\text{Al}_2\text{O}_3$  and  $\text{SiO}_2$ ) [4] or natural raw materials (e.g. talc, kaolinite, vermiculite, gibbsite, dolomite,

\* Corresponding author.

E-mail addresses: [karla.cech.barabaszova@vsb.cz](mailto:karla.cech.barabaszova@vsb.cz) (K. Čech Barabaszová), [jana.kupkova@vsb.cz](mailto:jana.kupkova@vsb.cz) (J. Kupková), [kamila.hrabovska@vsb.cz](mailto:kamila.hrabovska@vsb.cz) (K. Hrabovská), [sylva.holesova@vsb.cz](mailto:sylva.holesova@vsb.cz) (S. Holešová), [agnieszka.antonczyk@polsl.pl](mailto:agnieszka.antonczyk@polsl.pl) (A. Antończyk).

<sup>1</sup> ORCID code: 0000-0002-8667-4633

<sup>2</sup> ORCID code: 0000-0003-2278-593X

<sup>3</sup> ORCID code: 0000-0003-4563-6558

<sup>4</sup> ORCID code: 0000-0001-5233-5847

<sup>5</sup> ORCID code: 0000-0001-8093-4978

pyrophyllite [5] or industrial waste (e.g. fly ash [6,7]), granite sludge [3], silica fume [8]. Sintered cordierite ceramics contain indialite and mullite as the main phases, and corundum, spinel, forsterite, clinoenstatite, protoenstatite and cristobalite as secondary phases, together with a glassy phase [9]. The properties of the final ceramic products depend on the starting materials, firing conditions, the presence of impurities or additives and the processing conditions used in their preparation.

To improve the physical, mechanical and electrical properties of the resulting ceramic cordierite materials, the different additives, mainly in form of oxides, are used. The positive effect of many different oxide additives ( $\text{TiO}_2$ ,  $\text{ZrO}_2$ ,  $\text{ZnO}$ ,  $\text{SrO}$ ,  $\text{B}_2\text{O}_3$ ,  $\text{CuO}$ ) on the densification of cordierite ceramics has been tested [1,10]. Oxides such as  $\text{TiO}_2$ ,  $\text{ZrO}_2$  and  $\text{Fe}_2\text{O}_3$  caused the decrease of glass transition temperatures in cordierite ceramics [11]. Adding  $\text{ZnO}$  to pre-ceramic mixtures at different concentrations caused the formation of  $\mu$ - or  $\alpha$ -cordierite and gahnite ( $\text{ZnAl}_2\text{O}_4$ ) after sintering [12,13]. Cordierite ceramics obtained by doping with different concentrations of  $\text{ZnO}$  (from 1.5 to 3.0 wt%) and sintering at a lower temperature (950 °C) appear to be promising electronic packaging materials [12]. Adding transition metal oxides ( $\text{CuO}$ ,  $\text{NiO}$  and  $\text{MnO}_2$ ) to cordierite matrices caused cordierite and spinel phases to form after sintering at 1200 °C or 1250 °C. Sadek et al., 2023 also studied the mechanical and electrical properties in addition to the phase composition. Ceramics doped with transition metal oxides ( $\text{CuO}$ ,  $\text{NiO}$  and  $\text{MnO}_2$ ) showed higher electrical conductivity than pure ceramics [14]. Sadek et al., 2024 successfully prepared cordierite-spinel composites by doping of  $\text{ZnO}$ ,  $\text{TiO}_2$  and  $\text{Fe}_2\text{O}_3$  into the cordierite structure [15]. Sutormina et al., 2014 modified the catalysts based on the cordierite framework structure using transition metal oxides ( $\text{MnO}_2$ ,  $\text{Fe}_2\text{O}_3$ ,  $\text{Co}_3\text{O}_4$ ,  $\text{NiO}$ , and  $\text{CuO}$ ).  $\text{MgO}$  was partially or completely substituted with above mentioned oxides in the cordierite structure. The  $\text{NiO}$  and  $\text{Co}_3\text{O}_4$  oxides exhibited similar effect. The cobalt ( $\text{Co}^{2+}$ ) and nickel ( $\text{Ni}^{2+}$ ) ions were not incorporated into the cordierite structures but formed the cobalt- ( $\text{CoAl}_2\text{O}_4$ ) and nickel- ( $\text{NiAl}_2\text{O}_4$ ) aluminum spinel phases at the expense of the cordierite phase, respectively. A small amount of  $\text{Fe}^{2+}$  ions was incorporated into the cordierite structure, while a greater amount existed as the  $\alpha$ - $\text{Fe}_2\text{O}_3$ . Some  $\text{Cu}^{2+}$  ions were partially incorporated into the cordierite structure, formed the copper-aluminum spinel ( $\text{CuAl}_2\text{O}_4$ ) and  $\text{CuO}$  crystallites located on the surface. Catalysts enriched in  $\text{MnO}_2$ , consisting of substituted cordierite with  $\text{Mn}_2\text{O}_3$  on their surface appear to be a promising material for the industrial oxidation of ammonia [16]. Li et al., 2022 investigated the effect of introducing by  $\text{Fe}_3\text{O}_4$  as the functional additive on magnetic properties of porous cordierite ceramic. The authors looked for a way to decrease the synthesis temperature of cordierite ceramics while also imparting magnetism to the ceramics. Porous cordierite ceramics were prepared using the foam gel-casting method from  $\text{MgO}$ ,  $\text{Al}_2\text{O}_3$ ,  $\text{SiO}_2$  and  $\text{Fe}_3\text{O}_4$  powders. In addition to the main cordierite phase,  $\text{Mg-Al-Fe}$  spinel and  $\alpha$ - $\text{Fe}_2\text{O}_3$  were identified in the final ceramic samples [17].

Materials such as alumina, cordierite and mullite are often used to support ceramic membranes. Sintered  $\text{Al}_2\text{O}_3$  is the main material used for commercialized porous ceramic membrane support. Porous cordierite is a promising candidate for ceramic support, primarily due to its low fabrication cost, excellent resistance to thermal shock and good resistance to thermal alkali solutions [18,19]. The nature and structure of the supports can affect the membrane quality [19].

In general, the main concerns in the production of ceramic materials are reducing production costs and lowering the sintering temperature. Therefore, attention is focused primarily on natural, environmentally friendly raw materials. Depending on the composition of the initial pre-ceramic mixtures and the additives and technologies applied, cordierite ceramics with different microstructures and densities can be produced. Compared to previous work reported on  $\text{CuO}$  or  $\text{CoO}$  modified ceramic systems, the fundamental innovation is the measurement of the surface properties of the prepared doped particles based on the zeta potential and at the same time the optimal concentration of the metal oxide

nanoparticles used.

Two types of nanoparticles (copper oxide  $\text{CuO}$  and cobalt oxide  $\text{CoO}$ ) at different concentrations were used as nanostructured fillers to prepare cordierite nanocomposite particles. The main aim of the study was to determine the effect of the concentration of the nanoparticles and their different melting temperatures on the formation of the cordierite phase and whether these factors influence the morphology and size of the cordierite particles produced by grinding and sintering. Another objective was to identify appropriate nanoparticles concentration to ensure the thermal stability and magnetic properties of the ceramic nanocomposite particles. In general, studies dedicated to the magnetic properties of cordierite ceramics are rare because it typically exhibits diamagnetic behavior [20]. Modification of the ceramics is most often achieved using  $\text{Fe}_3\text{O}_4$  nanoparticles [16] or various types of ferrites [21], with the aim of obtaining functional materials that usually display superparamagnetic properties. The magnetic behavior in cordierite ceramics systems modified with  $\text{CoO}$  and  $\text{CuO}$  nanoparticles has not yet been discussed in the literature.

## 2. Experimental samples and characterisation methods

### 2.1. Cordierite nanocomposite particles

The initial cordierite particles were prepared using a mechano-chemical method from mixture of natural clay mineral particles (<40  $\mu\text{m}$ , 99% purity) and aluminum oxide particles (from Sigma Aldrich, <40  $\mu\text{m}$ ). Vermiculite particles from Brazil (12 wt%), kaolinite particles from Czech Republic (45 wt%) and talc particles from Egypt (30 wt%) were weighted (with aluminum oxide particles, Sigma Aldrich, <40  $\mu\text{m}$ ) in the stoichiometric ratio on their oxides corresponding to the cordierite composition  $2\text{MgO} \cdot 2\text{Al}_2\text{O}_3 \cdot 5\text{SiO}_2$  and ground in a planetary ball mill (Fritsch, Pulverisette 7) for 15 min in an agate milling vessel containing three agate balls at a rotation speed of 350 rpm. The prepare pre-ceramic mixtures were then sintered in a muffle furnace at 1320 °C for 1.5 h with heating rate 5°/min and natural cooling. After sintering, the ceramic samples were ground again in a planetary ball mill under the same conditions. The original cordierite particle sample was named C.

The modified cordierite nanocomposite particles were prepared under the same conditions as the initial C particles, except that different concentrations (1.5, 2.5, 3.5 and 5.5 wt%) of copper oxide ( $\text{CuO}$ ) or cobalt oxide ( $\text{CoO}$ ) nanoparticles (both purchased from Sigma Aldrich, 50 nm and 99.95% purity) were added to the mixture. The concentration of aluminum oxide particles (11.5, 10.5, 9.5 and 7.5 wt%) was reduced by adding  $\text{CuO}$  or  $\text{CoO}$  nanoparticles in adequate amounts, to maintain the input ratio of clay components and achieve the stoichiometric composition of the cordierite phase. The cordierite nanocomposite particles were labelled C1.5\_CuO, C2.5\_CuO, C3.5\_CuO and C5.5\_CuO, and C1.5\_CoO, C2.5\_CoO, C3.5\_CoO and C5.5\_CoO, respectively.

### 2.2. Evaluation methods

The morphology of the initial cordierite particles and cordierite nanocomposite particles was investigated using the scanning transmission electron microscope (JEOL JSM-7610F Plus, JEOL Ltd., Japan). The experimental powder samples were placed on aluminum targets and coated with a 25 nm layer of gold to protect conductivity and electrical charging during microscopic observation. SEM images were obtained using a secondary electron detector (SE, LEI).

The particle size (PS) was determined using the HORIBA Laser diffraction particle size analyser LA-950 instrument (Kyoto, Japan). The PS analyses were performed with the refractive indices 1.45 (for ceramic particles) and 1.33 (for water). Particle size distributions were evaluated via the Origin software.

The specific surface area (SSA) were measured at the liquid nitrogen atmosphere by means of Thermo Scientific Surfer (Milan, Italy). Before measurements, the samples were degassed under vacuum ( $10^{-6}$  bar) at

90 °C for 24 h. SSA was calculated using the Brunauer-Emmett-Teller (BET) isotherm.

Zeta-potential ( $\zeta$ -potential) was measured by a nanoparticle analyzer HORIBA Nanopartica SZ-100 (Kyoto, Japan) equipped with a micro-processor unit to directly calculate the  $\zeta$ -potential. The  $\zeta$ -potential values was calculated from the Smoluchowski equation.

The X-ray powder diffraction (XRD) analysis for the phase composition was performed using a RIGAKU Ultima IV diffractometer with a scintillation detector, CuK $\alpha$  radiation source, NiK $\beta$  filter and a Bragg–Brentano arrangement. The samples were measured at ambient atmospheric pressure by using the reflection mode (under the conditions 40 kV, 40 mA, 2 °/min and 0.1 step). The database used to obtain the qualitative phase analysis was ICDD PDF-2/Release 2022. The crystallite size ( $L_c$ ) of spinel phases CoAl<sub>2</sub>O<sub>4</sub> or CuAl<sub>2</sub>O<sub>4</sub> in the prepared nanocomposites was calculated based on (311) reflection (about 36.6° 2 $\theta$ ) according to the Scherrer's equation [22].

The chemical composition was obtained from elemental analysis using X-ray fluorescence spectroscopy (XRF) Supermini200 wavelength dispersive X-ray fluorescence spectrometer (RIGAKU, Japan). Powder samples were poured freely into polyethylene cups with thin Mylar films.

The thermogravimetric analysis (TGA) was performed at temperatures from 30 to 80 °C at heat rate of 10 °C/min in argon atmosphere (flow 50 ml/min). By this analysis technique was used to investigate thermal stability and degradation of the samples. The TGA tests were performed using Sestys Evolution (Setaram, France).

The magnetization of the powders was detected using a VSM EZ9 MicroSense vibrating magnetometer. The sample placed in the external magnetic field generated by the electromagnet induces a voltage which is sensed by the detection coils and whose magnitude is directly proportional to its mass magnetization. The measured magnetization curves at room temperature show the dependence of the mass magnetization on the strength of the external magnetic field. Maximal applied magnetic field was  $\pm 1600$  kA/m. Due to weak magnetic response of the samples the contribution of diamagnetic sample holder was subtracted from the

curves. A Sartorius LE 225D analytical balance was used to measure the weight of the powder samples.

### 3. Results and discussion

#### 3.1. The structural and particle characteristics of cordierite particles

Changes in the morphology of the initial cordierite particles (C) and the cordierite nanocomposite particles that were modified using different metal oxide nanoparticles were investigated using a scanning electron microscope (SEM). The SEM images are shown in Fig. 1. Fig. 2 shows the particle size distributions (PSD) in volume content the evaluated particle sizes (mode diameters) are listed in Table 1. The particle surface characteristics, such as the specific surface area and  $\zeta$ -potential values, are also listed in Table 1.

The initial cordierite particles (C) exhibited an irregular shape. They were predominantly composed of non-porous blocks with rounded edges measuring 4.47  $\mu\text{m}$  ( $d_{m2}$ ) and very fine grains on their surface. Locally, sharp edges of these particles were present, exhibiting a pointed shape. The sample volume contained very fine particles measuring 0.30  $\mu\text{m}$  ( $d_{m1}$ ), whose surfaces were in direct contact with the surfaces and edges of the C particles. Overall, the C particles had a relatively small specific surface area ( $\text{SSA} = 15.24 \text{ m}^2/\text{g}$ ), but the particles are the highest resistance to aggregation, as confirmed the  $\zeta$ -potential value of  $-44.3 \text{ mV}$ .

The cordierite nanocomposite particles retain their original bimodal character in terms of particle size distribution (Fig. 2), including particle size values ( $d_{m1}$  and  $d_{m2}$ ). Changes occur mainly in terms of surface area and non-aggregating abilities (as shown by  $\zeta$ -potential value).

The cordierite nanocomposite particles modified with CuO nanoparticles are composed of smooth surfaces with sharp edges. With increasing concentration of CuO nanoparticles, individual particle blocks become longer and the occurrence of very fine grains on their surfaces is minimized. While the particles of samples C1.5\_CuO and C2.5\_CuO are formed by crystalline particle blocks, the blocks of

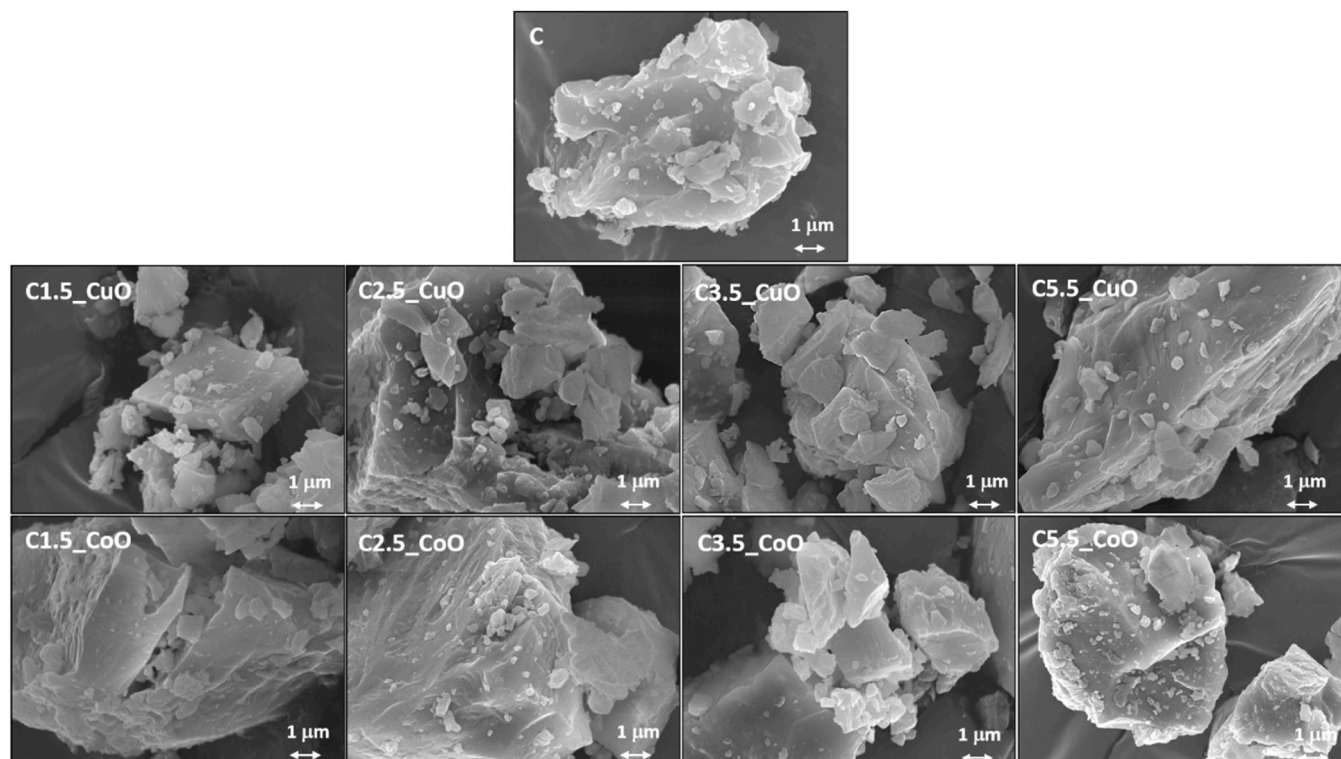
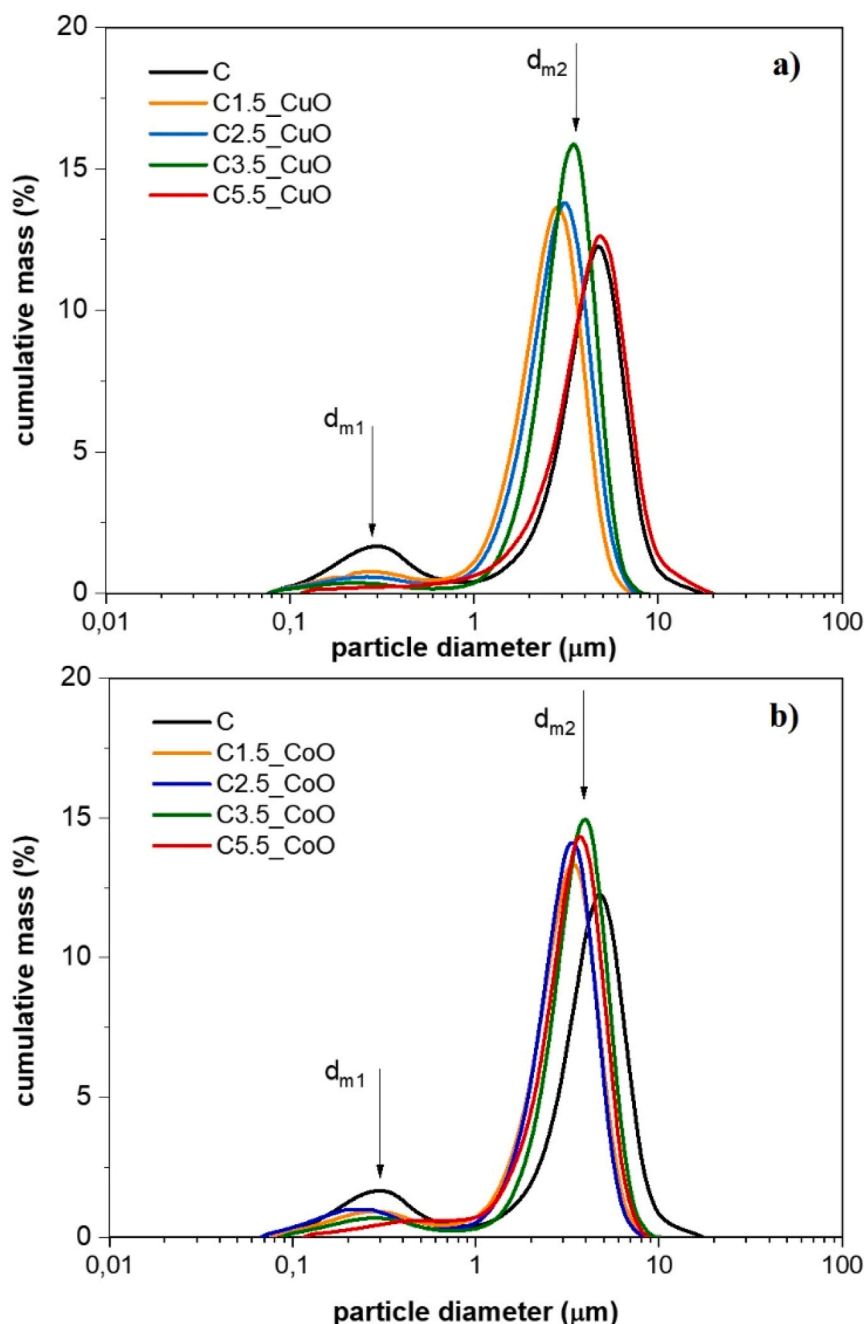


Fig. 1. SEM images of the initial cordierite particles (C) and cordierite nanocomposite particles doped with CuO or CoO nanoparticles at different concentrations.



**Fig. 2.** Particle size distributions (log-normal) of the a) initial cordierite (C) and cordierite nanocomposite particles doped with CuO nanoparticles at different concentrations; b) initial cordierite (C) and cordierite nanocomposite particles doped with CoO nanoparticles at different concentrations.

C3.5\_CuO and C5.5\_CuO samples are planar, and the particles are elongated, formed by a distinct lamellar structure. It can be assumed that CuO nanoparticles contribute to the plastic deformation of particles during ball milling due to their naturally malleable and ductile nature, where friction between the particles and the grinding media leads to the formation of elongated particles. The PSD curves (Fig. 2a) confirmed an increase in average size to  $3.41 \mu\text{m}$  for the C3.5\_CuO sample and  $5.12 \mu\text{m}$  for the C5.5\_CuO sample, while for the C5.5\_CuO sample, the fine particle fractions were not analyzed as separate objects. The SEM images show that the fine fractions are in direct contact with the edges of large particle blocks, thus forming particle agglomerates. In contrast, the very fine particle fractions ( $d_{m1} = 0.26 \mu\text{m}$ ) of the C1.5\_CuO and C2.5\_CuO samples exist independently throughout the entire volume of the samples. Structurally and surface stable cordierite nanocomposite

particles form the C3.5\_CuO sample. The nanocomposite particles achieve the highest specific surface area ( $\text{SSA} = 10.34 \text{ m}^2/\text{g}$ ), the highest volume fraction of particles of average value ( $d_{m1} = 3.41 \mu\text{m}$ ) 15.8% and the highest resistance to aggregation ( $\zeta$ -potential value of  $-34.1 \text{ mV}$ ).

The bimodal PSD was measured for the cordierite nanocomposite particles modified with CoO nanoparticles (Fig. 2b). The finest particle fractions reached values of  $0.26 \mu\text{m}$  (or  $0.30 \mu\text{m}$ ,  $d_{m1}$ ), and the average particle sizes ( $d_{m2}$ ) ranged from  $2.98$  to  $3.91 \mu\text{m}$ , with these values increasing with increasing CoO nanoparticle concentration (Table 1). In the sample with the highest concentration of CoO nanoparticles (C5.5\_CoO), the finest particle fraction ( $d_{m1}$ ) was not analyzed, but the particles showed the highest specific surface area ( $\text{SSA} = 14.77 \text{ m}^2/\text{g}$ ) and high  $\zeta$ -potential value of  $-30.2 \text{ mV}$ . The SEM image shows that the finest fraction consists of compact particle clusters together with a larger



**Table 1**

Particle parameters of the initial cordierite particles (C) and cordierite nanocomposite particles doped with CuO or CoO nanoparticles at different concentrations -  $d_m$  (particle size, mode diameters), SSA (specific surface area) and  $\zeta$  ( $\zeta$ -potential).

Samples	$d_{m1}$ ( $\mu\text{m}$ )	$d_{m2}$ ( $\mu\text{m}$ )	SSA ( $\text{m}^2/\text{g}$ )	$\zeta$ (mV)
C	0.30	4.47	15.24	$-44.3 \pm 0.8$
C1.5_CuO	0.26	2.98	7.34	$-34.7 \pm 3.2$
C2.5_CuO	0.26	2.98	1.77	$-34.3 \pm 2.1$
C3.5_CuO	0.23	3.41	10.34	$-34.1 \pm 2.0$
C5.5_CuO	-	5.12	3.35	$-25.2 \pm 1.7$
C1.5_CoO	0.30	2.98	9.95	$-30.1 \pm 2.7$
C2.5_CoO	0.26	3.41	9.01	$-29.0 \pm 1.9$
C3.5_CoO	0.30	3.91	8.44	$-26.1 \pm 0.9$
C5.5_CoO	-	3.91	14.77	$-30.2 \pm 1.6$

fraction ( $d_{m2}$ ) - agglomerates, with the particles in contact with each other face-to-face. PSD curves showed that mechanical preparation of nanocomposite particles doped with CoO nanoparticles led to a reduction in the average particle size ( $d_{m2}$ ) to 2.98  $\mu\text{m}$  (C1.5\_CoO) for all samples compared to the original undoped C particles ( $d_{m2} = 4.47 \mu\text{m}$ ). The morphology of C\_CoO nanocomposite particles consists of crystalline blocks of uniform shapes. The particles had rounded edges, with visible fractures in regularly repeating layers on these edges. It can be assumed that CoO nanoparticles contribute to the strengthening of cordierite nanocomposite particles, which break because of their preparation by grinding.

The measured values of  $\zeta$ -potential and specific surface area (SSA) of cordierite nanocomposite particles show that the presence of very fine nanometric fractions leads to an increase in these values for both CuO and CoO nanoparticles, with a limiting concentration of 3 wt%.

### 3.2. X-ray diffraction and X-ray fluorescence analysis

Figs. 3 and 4 show the measured XRD patterns of the original cordierite and cordierite nanocomposite particles. All synthesized cordierite nanocomposite particles and original cordierite particles contained a hexagonal high-temperature form of cordierite - indialite (In; PDF card No. 01-082-1884) as a main crystalline phase. Typical

intensive reflections for indialite are in the positions  $2\theta = 10.38^\circ$ ,  $21.66^\circ$ ,  $26.28^\circ$ ,  $28.36^\circ$  and  $29.41^\circ$ . The secondary phases identified in original cordierite particles (C) were spinel  $\text{MgAl}_2\text{O}_4$  (S; PDF card No. 00-021-1152) and corundum (C; PDF card No. 00-046-1212).

The addition of some amount of metal oxides CuO or CoO caused the formation of spinel-type oxides  $\text{CuAl}_2\text{O}_4$  (PDF card No. 01-073-1958) (Fig. 3) or  $\text{CoAl}_2\text{O}_4$  (PDF card No. 01-082-2251) (Fig. 4), respectively. The reflections typical for spinel-type oxides were in the positions corresponding to the interlayer space distances  $d = 0.287 \text{ nm}$ ,  $d = 0.245 \text{ nm}$ ,  $d = 0.203 \text{ nm}$  and  $d = 0.143 \text{ nm}$ . At higher temperatures, clay minerals such as talc, kaolinite and vermiculite, transform to the new crystalline phases. Kaolinite changes to metakaolinite at  $450\text{--}700^\circ\text{C}$ , at  $930\text{--}980^\circ\text{C}$  recrystallizes to Si-Al spinel and at  $1200\text{--}1250^\circ\text{C}$  to mullite and cristobalite. Talc transforms to enstatite and cristobalite at  $800\text{--}900^\circ\text{C}$ . Vermiculite crystallizes to the enstatite [2]. At higher temperature (about  $1040^\circ\text{C}$ ), spinel reacts with cristobalite and at about  $1350^\circ\text{C}$  form cordierite [23]. Generally, divalent cations (Me:  $\text{Ni}^{2+}$ ,  $\text{Cu}^{2+}$ ,  $\text{Co}^{2+}$ ) react at low temperatures ( $500\text{--}1000^\circ\text{C}$ ) with alumina and form corresponding metal aluminates ( $\text{MeAl}_2\text{O}_4$ ) with spinel structure. [24,25] Around  $1050^\circ\text{C}$ , CuO decomposes to  $\text{Cu}_2\text{O}$  and Cu ions can react with metakaolinite matrix which led to the formation of copper aluminate [26]. The formation of copper aluminate was accelerated due to copper ions having higher diffusivity and reactivity towards alumina sublayer [27]. The similar situation occurs when CoO is used in pre-ceramic cordierite mixtures. Incorporation of cobalt ions into the aluminosilicate materials led to the formation of cobalt aluminate [27]. It can be assumed that  $\text{Cu}^{2+}$  and  $\text{Co}^{2+}$  ions with a smaller radius ( $\text{Cu}^{2+}$  0.73 Å and  $\text{Co}^{2+}$  0.70 Å [16]) are not incorporated into the cordierite structure because no shift of diffraction reflections is observed but form spinel-type oxides.

The  $\text{CuAl}_2\text{O}_4$  crystallite sizes (Lc) in Table 2, calculated according to Scherrer's equation based on (311) reflection, gradually increases from 24 nm for C1.5\_CuO to 38 nm for C5.5\_CuO. Simultaneously, the FWHM values (Table 2) decrease from  $0.38^\circ$  to  $0.253^\circ$  in cordierite composites doped with CuO nanoparticles, which corresponds to crystallite growth. In the case of  $\text{CoAl}_2\text{O}_4$ , the crystallite sizes (Lc) derived from the (311) reflection, range from 29 to 34 nm (Table X). The  $\text{CoAl}_2\text{O}_4$  crystallite size (Lc) for sample C1.5\_CoO is 29 nm, while other samples exhibit slightly higher Lc values around 33 nm.

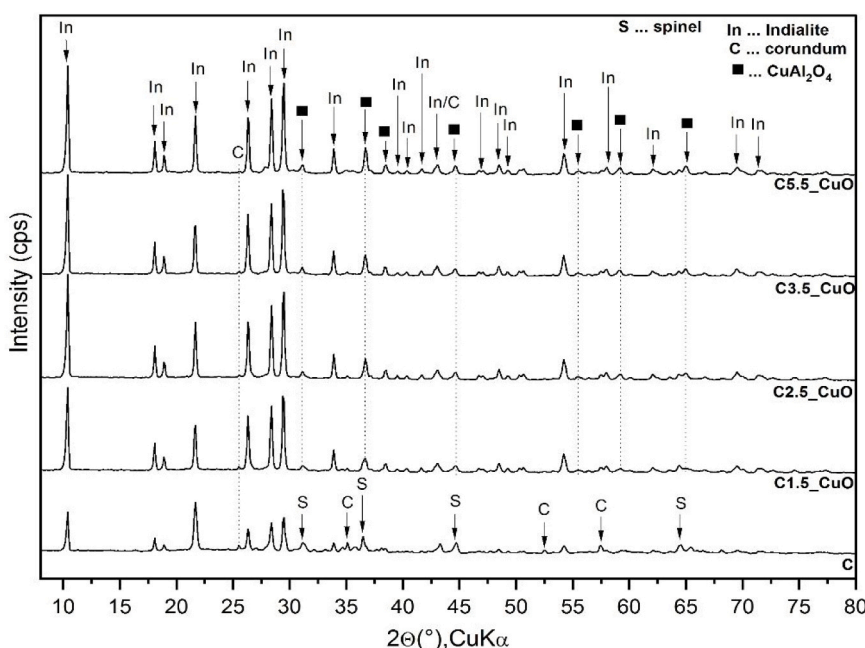


**Fig. 3.** XRD patterns of the initial cordierite particles (C) and cordierite nanocomposite particles doped with CuO nanoparticles.

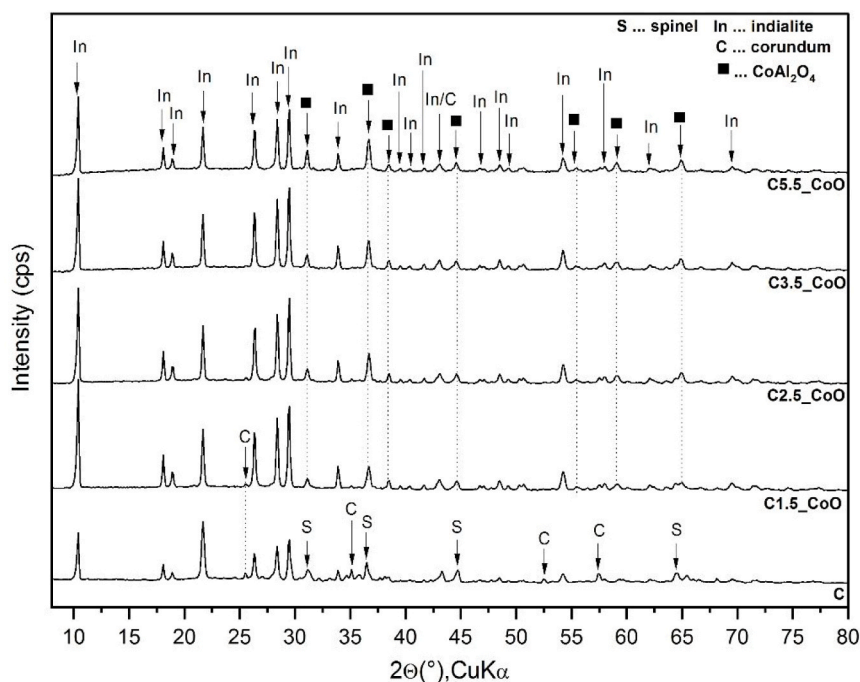


Fig. 4. XRD patterns of the initial cordierite particles (C) and cordierite nanocomposite particles doped with CoO nanoparticles.

Table 2

The XRD data ( $2\theta$ ,  $d$ -spacing, FWHM) for (311) reflection and calculated crystallite sizes (Lc) of spinel phases  $\text{CoAl}_2\text{O}_4$  or  $\text{CuAl}_2\text{O}_4$  of cordierite samples doped with CuO and CoO nanoparticles.

Samples	$2\theta$ (°)	$d(311)$ (nm)	FWHM (°)	Lc (nm)
C1.5_CuO	36.66	0.245	0.38	24
C2.5_CuO	36.69	0.245	0.30	31
C3.5_CuO	36.68	0.245	0.26	37
C5.5_CuO	36.72	0.245	0.253	38
C1.5_CoO	36.68	0.245	0.32	29
C2.5_CoO	36.68	0.245	0.28	34
C3.5_CoO	36.66	0.245	0.286	33
C5.5_CoO	36.65	0.245	0.276	34

The Table 3 summarizes the chemical composition of the initial cordierite (C) and cordierite ceramics doped by transition metal oxides CuO or CoO after sintering at 1320 °C. The theoretical composition of cordierite is as follows: 13.7 wt% of MgO, 51.4 wt% of  $\text{SiO}_2$  and 34.9 wt % of  $\text{Al}_2\text{O}_3$  [2]. The natural clay minerals (kaolinite, talc and vermiculite) used in pre-ceramics mixtures contain, in addition to the three previously mentioned oxides, also other oxides such as CaO,  $\text{K}_2\text{O}$ ,  $\text{Na}_2\text{O}$ ,  $\text{Fe}_2\text{O}_3$  and  $\text{TiO}_2$ . The XRF analysis confirmed that Si, Al and Mg are the main components for the cordierite ceramics and their contents in the form of oxides were: MgO 11.00 wt%,  $\text{SiO}_2$  48.3 wt% and  $\text{Al}_2\text{O}_3$

35.80 wt% for initial cordierite particles (C). The lower  $\text{SiO}_2$  and MgO contents, in comparison to theoretical cordierite, are caused mainly due to the presence of impurity oxides such as  $\text{Fe}_2\text{O}_3$  (2.48 wt%), CaO (1.81 wt%) and  $\text{K}_2\text{O}$  (1.13 wt%). In cordierite nanocomposite particles enriched with CuO or CoO nanoparticles, the  $\text{SiO}_2$ ,  $\text{Al}_2\text{O}_3$  and MgO are still as the main components. The CuO content of sintered ceramic particles ranges from 1.56 to 6.42 wt%, and the CoO content ranges from 1.80 to 5.29 wt%. In both cases of cordierite nanocomposite particles enriched with metal nanoparticles, the content of  $\text{K}_2\text{O}$ , CaO and  $\text{Fe}_2\text{O}_3$  decreased slightly. The cordierite nanocomposite particles doped with CuO showed the gradual decrease in  $\text{SiO}_2$  content (the lowest  $\text{SiO}_2$  value of 43.90 wt% for C5.5\_CuO sample). This confirms that, as the CuO concentration increases,  $\text{SiO}_2$  positions are predominantly replaced in the structure.

In contrast, cordierite nanocomposite particles enriched with CoO nanoparticles showed a significant decrease in MgO concentration from the original 11.9 wt% (C sample) to a concentration in the range of 9.73–8.62 wt%, with MgO concentration decreasing as CoO nanoparticle concentration increased. It can be assumed that  $\text{Co}^{2+}$  cations replace  $\text{Mg}^{2+}$  positions during heat treatment (sintering) and simultaneously replace positions in the spinel phase (see XRD patterns), which is consistent with [16,28]. This fact may also contribute to the formation of crystalline-oriented blocks of nanocomposite C\_CoO particles.

Table 3

Chemical composition of the initial cordierite particles (C) and cordierite nanocomposite particles doped with CuO or CoO nanoparticles after sintering at 1320 °C.

Samples	MgO (wt%)	$\text{Al}_2\text{O}_3$	$\text{SiO}_2$	$\text{K}_2\text{O}$	CaO	$\text{Fe}_2\text{O}_3$	CuO	CoO
C	11.00	35.80	48.30	1.13	1.81	2.48	-	-
C1.5_CuO	10.90	34.30	47.30	1.03	1.63	2.10	1.56	-
C2.5_CuO	11.40	34.30	46.30	0.94	1.46	1.94	2.40	-
C3.5_CuO	11.60	34.10	45.50	0.92	1.43	2.00	3.41	-
C5.5_CuO	11.50	33.00	43.90	0.90	1.42	1.92	6.42	-
C1.5_CoO	9.73	34.20	48.10	1.09	1.74	2.26	-	1.80
C2.5_CoO	9.18	33.70	47.00	1.03	1.64	2.12	-	3.14
C3.5_CoO	8.98	33.70	46.70	1.04	1.67	2.09	-	4.10
C5.5_CoO	8.62	32.80	47.00	1.07	1.70	1.86	-	5.29

### 3.3. Thermal and thermogravimetric analysis

Thermal analysis of pre-mixtures of cordierite ceramic samples was performed using the thermal analyzer Setsys 24 Evolution Setaram (Setaram, France). The thermal curves were recorded under following conditions: air atmosphere (75 ml/min), final temperature 1200 °C, heating rate 10 °C/min and sample mass about 5 mg. The parameters such as final weight loss ( $\Delta m$ ), the onset, offset temperatures and the temperature of maximum weight loss  $T_{\max}$  were determined from thermal curves.

Based on the thermal analysis of pre-mixtures of cordierite ceramic samples we wanted to simulate and characterize chemical/structural changes at samples under thermal treatment. Fig. 5 shows TG and dTG curves of these samples. Thermal data are concluded at Table 4.

From dTG curve (Fig. 5a) of starting pre-mixture of initial cordierite ceramic sample C we can observe exothermic peak at 502.6 °C corresponding to transformation of kaolinite to metakaolinite. The second peak at 914.4 °C can be caused by a combination of several phenomena, when vermiculite crystallizes into enstatite, talc changes into enstatite and cristobalite, and recrystallization of  $\gamma$ - $\text{Al}_2\text{O}_3$  and metakaolinite into Si-Al spinel occurs [2].

For the samples doped with metal oxides CuO or CoO, we observed also exothermic peak around 500 °C corresponding to transformation of kaolinite to metakaolinite. The second peak, unlike the original C sample (914.4 °C), was in the case of higher CuO content in the sample C5.5\_CuO shifted to lower value 857.3 °C, on the other hand in the case of CoO (C5.5\_CoO), the temperature was higher (921.1 °C). In the systems CuO or CoO and  $\text{Al}_2\text{O}_3$ , the formation about 80% of copper or cobalt aluminate ( $\text{MeAl}_2\text{O}_4$ ) occurred on heating to 1000 °C [24,29].

For these doped samples, we observed one more temperature phenomenon in the temperature range 1097 – 1164 °C. Based on Tsuchida et al., 1984  $\text{CuAl}_2\text{O}_4$  decomposed to  $\text{CuAlO}_2$ ,  $\text{Al}_2\text{O}_3$  and  $\text{O}_2$  in the temperature range 1130 – 1230 °C [29]. Around 1100 °C, CuO and CoO decomposed and Cu and Co ions react with metakaolinite matrix which led to the formation of copper or cobalt aluminates ( $\text{MeAl}_2\text{O}_4$ ,  $\text{MeAlO}_2$ ) [24,29].

**Table 4**

Thermal data ( $\Delta m$ ,  $T_{\max}$ ) of the initial cordierite particles (C) and cordierite nanocomposite particles doped with CuO or CoO nanoparticles.

Samples	$\Delta m$ (%)	$T_{\max 1}$ (°C)	$T_{\max 2}$ (°C)	$T_{\max 3}$ (°C)
C	9.06	502.6	914.4	-
C1.5_CuO	8.96	503.1	913.7	1163.8
C5.5_CuO	7.84	501.7	857.3	1132.6
C1.5_CoO	8.23	502.2	915.7	1097.4
C5.5_CoO	8.43	504.7	921.1	1162.1

### 3.4. Magnetic properties

Room temperature magnetization curves of investigated powder samples are shown in Figs. 6 and 7 and corresponding magnetic parameters are summarized in Table 5.

A weak magnetic response was observed for pure cordierite ceramics powder (insets of Figs. 6b and 7b). Because the oxides MgO,  $\text{Al}_2\text{O}_3$ ,  $\text{SiO}_2$ ,  $\text{K}_2\text{O}$ , and CaO detected from the XRF measurements are diamagnetic, the small magnetization value at a magnetic field of 1600 kA/m ( $M_{1600} \approx 0.0475 \text{ Am}^2/\text{kg}$ ) and a coercive field ( $H_c \approx 4.7 \text{ kA/m}$ ) are probably related to the low amount of  $\alpha$ - $\text{Fe}_2\text{O}_3$  (2.48 wt%) formed in the ceramics after annealing at 1320 °C. The non-zero hysteresis at low magnetic fields, followed by a slight curvature and then a linear increase in magnetization at higher fields, is consistent with the presence of hematite particles whose interiors exhibit antiferromagnetic behavior and possess uncompensated magnetic moments on their disordered particle surfaces.

Room-temperature magnetization curves of cordierite ceramics doped by CoO nanoparticles with different concentrations are presented in Fig. 6. Pure CoO nanoparticles (subplot 6a) exhibit strong ferromagnetic behaviour with  $M_{1600} = 8.90 \text{ Am}^2/\text{kg}$  and  $H_c = 11.17 \text{ kA/m}$ . However, after annealing at 1320 °C the magnetization markedly decreased and exhibited a linear dependence on an applied magnetic field with nearly zero remanence and coercive field. For CoO nanoparticles, it can generally be assumed that higher temperature leads to particle growth, which reduces the influence of the surface and results in a significant decrease in ferromagnetism. According to the literature the annealing of CoO at temperatures above 500 °C yields  $\text{Co}_3\text{O}_4$ , what is

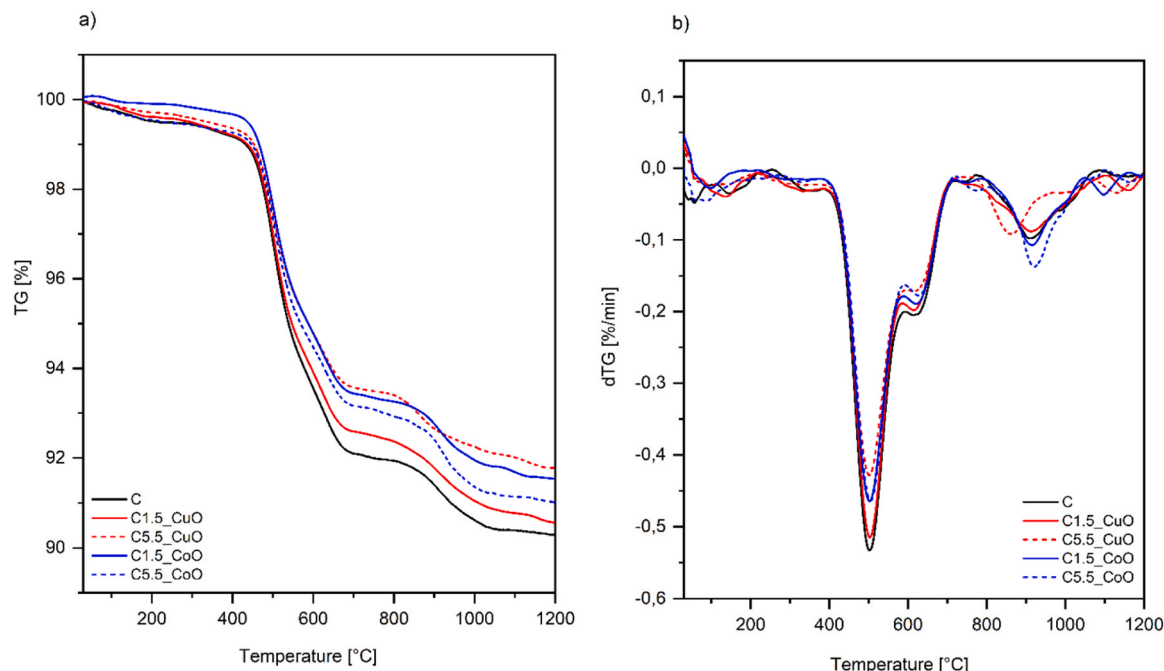


**Fig. 5.** TGA and dTG curves of the initial cordierite particles (C) and cordierite nanocomposite particles doped with CuO or CoO nanoparticles.

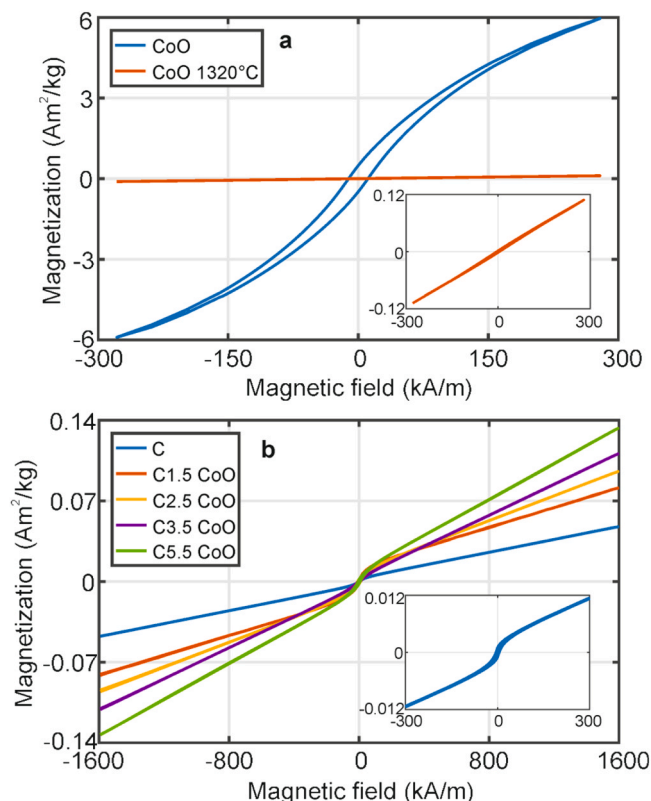


**Fig. 6.** Room temperature magnetization curves of (a) pure CoO nanoparticles in as-cast state and after annealing at 1320 °C for 1.5 h and (b) initial cordierite particles (C), detail in inset) and cordierite nanocomposite particles doped with CoO nanoparticles with different concentrations (1.5, 2.5, 3.5 and 5.5 wt%).

black, antiferromagnetic powder substance [30].

Therefore, the magnetization curves of cordierite ceramics doped with various concentrations of CoO have two contributions - magnetic reversal at low magnetic fields originating from pure cordierite ceramics and a linear contribution at higher magnetic fields coming from annealed CoO nanoparticles, see Fig. 6b. As a result, the magnetic parameter  $M_{1600}$  systematically increases with the content of doped nanoparticles, whereas the remanent magnetization  $M_r$  and coercive field  $H_c$  remain essentially unchanged due to the similar particle sizes of the samples.

The magnetic behaviour of the samples doped with CuO nanoparticles differs, as shown in Fig. 7. Pure CuO nanoparticles (subplot, Fig. 7a) appear to exhibit a combination of dominant antiferromagnetic (higher magnetic fields) and weak ferromagnetic (lower magnetic fields) behaviour with  $H_c = 14.36$  kA/m and  $M_r = 0.0012$  Am<sup>2</sup>/kg. Such room-temperature magnetic properties are in good agreement with a previous study [31]. In contrast to CoO nanoparticles, annealing at 1320 °C enhances the ferromagnetic contribution of CuO nanoparticles, as evidenced by its manifestation at low magnetic fields. The reason is the annealing temperature of 1320 °C, which is close to the melting point of CuO (1326 °C). This leads to a change in the structure of the entire system and to the formation of a magnetically soft phase with a coercive field approximately fourteen times smaller than that of the original CuO nanoparticles.

The magnetization curves of cordierite ceramics doped with various concentrations of CuO again exhibit two contributions (subplot, Fig. 7b) – a magnetic reversal at low magnetic fields originating mainly from the CuO nanoparticles and a linear contribution at higher magnetic fields arising from both the CuO nanoparticles and the cordierite ceramics. Due to the stronger ferromagnetic contribution, the remanence is approximately three to four times higher than in the original ceramics

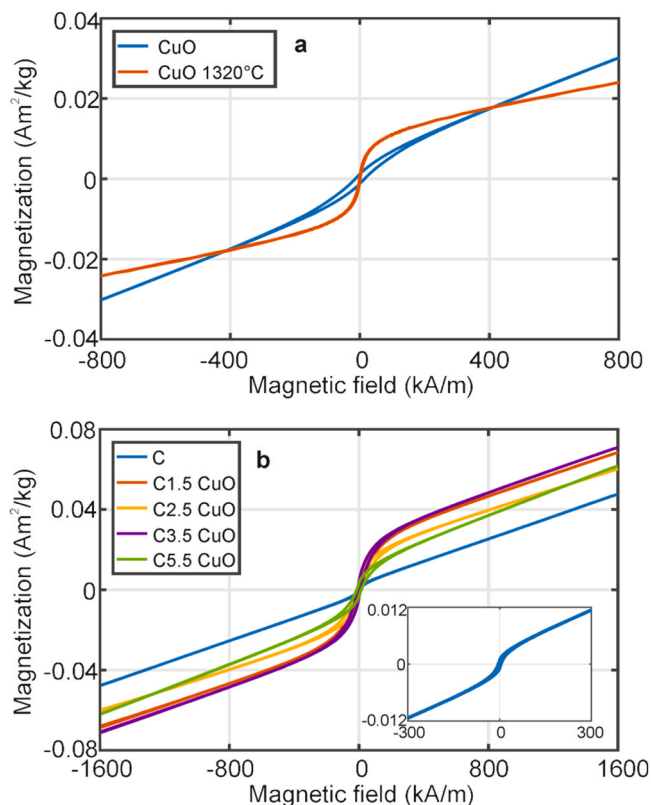


**Fig. 7.** Room temperature magnetization curves of (a) pure CuO nanoparticles in as-cast state and after annealing at 1320 °C for 1.5 h and (b) initial cordierite particles (C), detail in inset) and cordierite nanocomposite particles doped with CuO nanoparticles with different concentrations (1.5, 2.5, 3.5 and 5.5 wt%).

**Table 5**

Magnetic parameters of the initial cordierite particles (C) and cordierite nanocomposite particles doped with CuO or CoO nanoparticles, obtained from magnetization curves:  $M_{1600}$  - magnetization at magnetic field 1600 kA/m,  $M_r$  - remanent magnetization,  $H_c$  - coercive field.

Samples	$H_c$ (kA/m)	$M_r$ (Am <sup>2</sup> /kg)	$M_{1600}$ (Am <sup>2</sup> /kg)
C	4.70	0.0009	0.0475
CuO	14.36	0.0012	0.0550
CuO 1320 °C	1.037	0.0006	0.0359
C1.5_CuO	6.15	0.0043	0.0676
C2.5_CuO	10.40	0.0033	0.0596
C3.5_CuO	9.80	0.0039	0.0705
C5.5_CuO	14.20	0.0033	0.0616
CoO	11.17	0.4891	8.9027
CoO 1320 °C	4.15	0.0019	0.5910
C1.5_CoO	4.78	0.0010	0.0814
C2.5_CoO	9.53	0.0020	0.0955
C3.5_CoO	7.97	0.0010	0.1110
C5.5_CoO	5.79	0.0018	0.1328

and in the ceramics containing CoO nanoparticles, while the values of coercive field reflect the increase in particle size with increasing CuO concentration. In contrast, the antiferromagnetic behaviour at higher magnetic fields and the values of magnetization at maximal applied magnetic field ( $M_{1600}$ ) remain stable and are practically independent of the CuO nanoparticle concentration. It appears that variations in the CuO nanoparticle concentration in the range of 1.5–5.5 wt% are not sufficient to significantly alter the magnetic response even at the highest magnetic fields of  $\pm 1600$  kA/m.

Cordierite nanocomposite particles doped with CuO and CoO nanoparticles exhibits weak magnetic response, which precludes their



application, for example, in magnetic separators requiring saturation magnetization of the order of several tens of  $\text{Am}^2/\text{kg}$ . The main limiting factor here is annealing at high temperatures exceeding  $1000^\circ\text{C}$ . However, the introduction of suitable magnetic components, such as  $\text{Fe}_3\text{O}_4$ , into a powdered sample of cordierite ceramics after its preparation can significantly improve its ferromagnetic properties [17].

#### 4. Conclusion

Ceramic cordierite nanocomposite particles doped with CuO or CoO nanoparticles were prepared using a combination of milling and sintering at  $1320^\circ\text{C}$ . Magnetic curves showing two contributions were detected for both nanocomposites. Systems doped with CoO nanoparticles exhibit poor magnetic reversal at low magnetic fields originating from initial cordierite ceramics, and a linear contribution at higher magnetic fields that increases systematically with the content of CoO nanoparticles. In ceramics doped with CuO nanoparticles, a stronger soft ferromagnetic response at low magnetic fields arises because the annealing temperature is close to the melting point, causing the system to undergo a complete structural transformation. In contrast, the antiferromagnetic contribution is weak, and no significant difference is observed between the magnetization curves for different CuO concentrations at higher magnetic fields. The addition of CoO nanoparticles led to a decrease in MgO and  $\text{Al}_2\text{O}_3$ , while CuO nanoparticles showed the decrease in  $\text{Al}_2\text{O}_3$  and  $\text{SiO}_2$  in cordierite nanocomposites. C3.5\_CuO cordierite nanocomposite particles were found to be the most surface stable in a direct consequence of the synergy between the electrostatic environment and the physical shape of the particle. They had an elongated shape, a  $\zeta$ -potential value of  $-34.1\text{ mV}$  and a specific surface area of  $10.34\text{ m}^2/\text{g}$ . The highest magnetization values in a  $1600\text{ kA/m}$  magnetic field were measured for C5.5\_CoO cordierite nanocomposite particles ( $M_{1600} = 0.1328\text{ Am}^2/\text{kg}$ ), consisting of uniform crystalline blocks with a specific surface area of  $14.77\text{ m}^2/\text{g}$  and a  $\zeta$ -potential value of  $-30.2\text{ mV}$ . TGA analysis of the pre-mixtures confirmed that CuO and CoO nanoparticles are incorporated into the spinel structure in the form of  $\text{MeAl}_2\text{O}_4$  at temperatures above  $900^\circ\text{C}$ . Further increase in temperature above  $1000^\circ\text{C}$  leads to decomposition of these spinel phases and the formation of so-called aluminates  $\text{MeAlO}_2$ .

#### CRedit authorship contribution statement

**Karla Čech Barabaszová:** Writing – review & editing, Writing – original draft, Project administration, Methodology, Investigation, Formal analysis, Conceptualization. **Jana Kupková:** Writing – original draft, Formal analysis. **Kamila Hrabovská:** Writing – original draft, Formal analysis. **Sylva Holešová:** Writing – review & editing, Writing – original draft, Formal analysis. **Agnieszka Antończyk:** Writing – review & editing.

#### Author contributions

K.Č.B., SEM morphology, PS, PSD, Zeta-potential and SSA measured and evaluated, writing original draft, revised and finalized the manuscript; Writing – review & editing, Writing – original draft, Visualization, Supervision, Methodology, Formal analysis, Conceptualization. J.K., XRD and XRF analysis and their evaluation and writing original draft. S.H., TGA analysis evaluated, writing original draft and revised the manuscript. K.H., magnetic properties measurement and evaluation and writing original draft. A.A., consulted the manuscript.

#### Funding

This research received no external funding.

#### Declaration of Competing Interest

The authors declare the following financial interests/personal relationships which may be considered as potential competing interests: Karla Čech Barabaszová reports financial support was provided by VSB-Technical University of Ostrava. If there are other authors, they declare that they have no known competing financial interests or personal relationships that could have appeared to influence the work reported in this paper.

#### Acknowledgments

This work was supported by the project No. CZ.02.01.01/00/22\_008/0004631 “Materials and technologies for sustainable development” within the Jan Amos Komenský Operational Program financed by the European Union and from the state budget of the Czech Republic and project No. CZ.10.03.01/00/22\_003/0000045 „CirkArena project” within the Operational Programme Just Transition under the aegis of the Ministry of the Environment of the Czech Republic.

Authors thank to L. Plesník for SEM micrographs and K. Škrlová for help with the mechanical processing of the experimental samples.

#### Data availability

The data that support the findings of this study are openly available in repository ZENODO at <https://zenodo.org/records/14644501> [32].

#### References

- [1] A. Chowdhury, S. Maitra, S. Das, A. Sen, G.K. Samanta, P. Data, Synthesis, properties and applications of cordierite ceramics, Part 1, *InterCeram, Int. Ceram. Rev.* 56 (2007) 18–22.
- [2] M. Valášková, Clays, clay minerals and cordierite ceramics – a review, *Ceram. Silik.* 59 (2015) 331–340.
- [3] H.E.H. Sadek, M.F. Zawrah, A.A. Gaber, H.A. Badr, A.M. El-Rafei, R.M. Khattab, Utilization of granite sludge for production of cordierite ceramics by direct coagulation casting, *Ceram. Int.* 47 (2021) 20187–20195, <https://doi.org/10.1016/j.ceramint.2021.04.025>.
- [4] H. Li, C. Li, L. Wu, Porous cordierite ceramics prepared by foam-gelcasting technique: phase evolution and properties, *J. Alloy. Compd.* 791 (2019) 690–699, <https://doi.org/10.1016/j.jallcom.2019.03.225>.
- [5] S. Tamborenea, A.D. Mazzoni, E.F. Aglietti, Mechanochemical activation of minerals on the cordierite synthesis, *Thermochim. Acta* 411 (2004) 219–224, <https://doi.org/10.1016/j.tca.2003.08.017>.
- [6] Y. He, W. Cheng, H. Cai, Characterization of  $\alpha$ -cordierite glass-ceramics from fly ash, *J. Hazard. Mater.* 120 (2005) 265–269, <https://doi.org/10.1016/j.jhazmat.2004.10.028>.
- [7] R. Goren, C. Ozgur, H. Gocmez, The preparation of cordierite from talc, fly ash, fused silica and alumina mixtures, *Ceram. Int.* 32 (2006) 53–56, <https://doi.org/10.1016/j.ceramint.2005.01.001>.
- [8] R.M. Khattab, A.M. El-Rafei, M.F. Zawrah, situ formation of sintered cordierite-mullite nano-micro composites by utilizing of waste silica fume, *Mater. Res. Bull.* 47 (2012) 2662–2667, <https://doi.org/10.1016/j.materresbull.2012.04.036>.
- [9] D.U. Tulyaganov, M.E. Tukhtaev, J.I. Escalante, M.J. Ribeiro, J.A. Labrincha, Processing of cordierite based ceramics from alkaline-earth-aluminosilicate glass, kaolin, alumina and magnesite, *J. Eur. Ceram. Soc.* 22 (2002) 1775–1782, [https://doi.org/10.1016/S0955-2219\(01\)00506-4](https://doi.org/10.1016/S0955-2219(01)00506-4).
- [10] W. Gao, J. Kanga, D. Zhao, J. Sia, X. Wua, Y. Yuea, Y. Qua, Z. Xiaoa, N. Zhang, A novel high  $Q \times f$  value glass-ceramic with ultra-low sintering temperature for ULTCC substrate application, *Ceram. Int.* 51 (2025) 65434–65445, <https://doi.org/10.1016/j.ceramint.2025.11.221>.
- [11] M. Valášková, Z. Klika, B. Novosad, B. Smetana, Crystallization and quantification of crystalline and non-crystalline phases in kaolin-based cordierites, *Materials* 12 (2019) 3104, <https://doi.org/10.3390/ma12193104>.
- [12] G. Chen, Effect of ZnO addition on properties of cordierite-based glass-ceramics, *J. Mater. Sci. Mater. Electron* 18 (2007) 1253–1257, <https://doi.org/10.1007/s10854-007-9283-8>.
- [13] K.Čech Barabaszová, J. Kupková, K. Škrlová, S. Študentová, Cordierite nanocomposite particles with addition of Zinc Oxide, *J. Comput. Theor. Nanosci.* 22 (2016) 691–694, <https://doi.org/10.1166/asl.2016.6902>.
- [14] H.E.H. Sadek, M. Zawrah, R. Khattab, H.H. Abo-Elmaged, Effect of CuO, NiO, MnO<sub>2</sub> and sintering temperature on the formation of cordierite-spinel composites processed by direct coagulation casting, *J. Mater. Sci. Mater. Electron* 34 (2023) 1196, <https://doi.org/10.1007/s10854-023-10594-5>.
- [15] H.E.H. Sadek, M.F. Zawrah, F. Abd-El-Raouf, Z.A. Abd El-Shakour, M.A. Taha, R. M. Khattab, Effect of ZnO, TiO<sub>2</sub> and Fe<sub>2</sub>O<sub>3</sub> on inhibition of spinel formation during cordierite fabrication: sinterability, physico-mechanical and electrical properties,

- J. Inorg. Organomet. Polym. Mater. 34 (2024) 1068–1080, <https://doi.org/10.1007/s10904-023-02750-5>.
- [16] E.F. Sutormina, L.A. Usupova, N.A. Kulikovskaya, A.V. Kuznetsova, N.A. Rudina, Catalysts based on cordierite modified with transition metal oxides, Kinet. Catal. 55 (2014) 656–664, <https://doi.org/10.1134/S0023158414050176>.
- [17] H. Li, C. Li, H. Jia, G. Chen, S. Li, K. Chen, Ch Wang, L. Qiao, Facile fabrication of cordierite-based porous ceramics, J. Adv. Ceram. 11 (2022) 1583–1595, <https://doi.org/10.1007/s40145-022-0631-1>.
- [18] Y. Dong, X. Feng, D. Dong, S. Wang, J. Yang, J. Gao, X. Liu, G. Meng, Elaboration and chemical corrosion resistance of tubular macro-porous cordierite ceramic membrane supports, J. Membr. Sci. 304 (2007) 65–75, <https://doi.org/10.1016/j.memsci.2007.06.058>.
- [19] L. Zhou, T. Wang, Q.T. Nguyen, J. Li, Y. Long, Z. Ping, Cordierite-supported ZSM-5 membrane: preparation and pervaporation properties in the dehydration of water–alcohol mixture, Sep. Purif. Technol. 44 (2005) 266–270, <https://doi.org/10.1016/j.seppur.2004.12.016>.
- [20] G. Kirat, M.A. Aksan, Observation of magnetic behavior at low temperature in the  $\text{Mg}_2\text{Al}_4\text{Si}_5\text{O}_{18}$  system, J. Alloy Compd. 577 (2013) 556–559, <https://www.sciencedirect.com/science/article/pii/S0925838813015624>.
- [21] Z. Yue, L. Li, J. Zhou, H. Zhang, Z. Ma, Z. Gui, Preparation and electromagnetic properties of ferrite–cordierite composites, Mater. Lett. 44 (2000) 279–283, <https://www.sciencedirect.com/science/article/pii/S0167577X00000458>.
- [22] P. Scherrer, Bestimmung der Größe und der inneren Struktur von Kolloidteilchen mittels Röntgenstrahlen, Nachr. Ges. Wiss. Gott. 2 (1918) 98–100.
- [23] A.A. Albhilil, M.T. Palou, J. Kozánková, Characterization of cordierite–mullite ceramics prepared from natural raw materials, Acta Chim. Slov. 6 (2013) 1–7, <https://doi.org/10.2478/ACS-2013-0001>.
- [24] S. Kurajica, E. Tkadlec, J. Schmauch,  $\text{CoAl}_2\text{O}_4$ –mullite composites prepared by sol-gel processes, J. Eur. Ceram. Soc. 27 (2007) 951–958, <https://doi.org/10.1016/j.jeurceramsoc.2006.04.127>.
- [25] D. Mazza, A. Delmastro, S. Ronchetti, Co, Ni, Cu aluminates supported on mullite precursors via a solid, J. Eur. Ceram. Soc. 20 (2000) 699–706, [https://doi.org/10.1016/S0955-2219\(99\)00196-X](https://doi.org/10.1016/S0955-2219(99)00196-X).
- [26] T. Martišius, R. Giraitis, Influence of copper oxide on mullite formation from kaolinite, J. Mater. Chem. 13 (2003) 121–124, <https://doi.org/10.1039/B206711K>.
- [27] J. Roy, N. Bandyopadhyay, S. Das, S. Maitra, Effect of copper ions on mullite formation from aluminosilicate precursor, Ceram. Silik. 54 (2010) 128–132.
- [28] A.E. Reda, F. Abd-El-Raouf, S.E. Ahmed, D.A. Abdel Aziz, R. Mahani, Sintering and dielectric behavior for doped cordierite by xCuO within  $\text{MgO}$  (1-x)– $\text{Al}_2\text{O}_3$ – $\text{SiO}_2$  ceramics, Mater. Chem. Phys. 243 (2020) 122616, <https://doi.org/10.1016/j.matchemphys.2019.122616>.
- [29] T. Tsuchida, R. Furuichi, T. Sukegawa, M. Furudate, T. Ishii, Thermoanalytical study on the reaction of the  $\text{CuO}$ – $\text{Al}_2\text{O}_3$  ( $\eta$ ,  $\gamma$  and  $\alpha$ ) systems, Thermochim. Acta 78 (1984) 71–80, [https://doi.org/10.1016/0040-6031\(84\)87134-8](https://doi.org/10.1016/0040-6031(84)87134-8).
- [30] K. Ekkehard, Magnetic structure of  $\text{CoO}$ , Symmetry 13 (2021) 1513, <https://doi.org/10.3390/sym13081513>.
- [31] F. Mbarek, I. Chérif, A. Chérif, J.M. Alonso, I. Morales, P. de la Presa, S. Ammar, Insights into the synthesis parameters effects on the structural, morphological, and magnetic properties of copper oxide nanoparticles, Materials 16 (2023) 3426, <https://doi.org/10.3390/ma16093426>.
- [32] K. Čech Barabaszová, J. Kupková, K. Hrabovská, S. Holešová, A. Antończyk, Correlation between CuO and CoO nanoparticles concentration and magnetic reversal in mechanochemically prepared cordierite ceramics, Zenodo (2025).